Chapter 5

Methods for recreating ILC backgrounds: Introduction and Method A

5.1 Introduction to the methods for recreating ILC backgrounds

Three methods were developed to be used at ESA to test the stripline response to backgrounds.

Method A, as described in detail throughout this chapter, uses the material of the FONT module (chapter 4) to create many secondaries in the region of the BPM and study the response of the BPM to them. The ESA electron beam was moved to positions on the front face of the module, the low-Z mask. It then interacts with the material of the module, which has radiation lengths, absolute lengths and apertures closely matching those of the ILC IR, generating many secondaries. By the z location of the BPM, most of the beam comprises secondaries (only 1% of the main beam survives to this point) allowing the study of the effect of low energy particles on the raw stripline and on the processed stripline signals.

Method B, as discussed in chapter 6, uses thin foils of aluminium a few metres upstream of the module to create a halo of electrons that interact with the module and shower in the material while allowing most of the main beam to continue through the beampipe. Secondaries are therefore present in the BPM region at the same time as the main beam signal. It is therefore possible to measure the beam position in the presence of backgrounds and, by removing the foils, compare this to the beam position in a clean environment, to see if there is a degradation in resolution.

Method C, as discussed in chapter 7, creates a wide, beampipe-filling spray beam of electrons using a thick radiator in the Beam Switch Yard (BSY) at the end of the SLAC linac. A momentum bite of this beampipe-filling spray can be transported with magnets to ESA, delivering a uniform distribution of electrons to the front face of the module (the low-Z mask). Using different momentum settings and different beam charge incident on the

thick radiator, it is possible to match the average energy and number distribution of the ILC backgrounds on the low-Z mask.

These methods are summarised in table 5.1.

5.2 Methods for creating spray: A

5.2.1 Overview

In the ILC simulations, the particles that hit the BPM striplines originated from the lip of the inner radius of the low-Z mask as shown in figure 3.26. To create backgrounds at ESA, the input beam for use with the FONT module was the ESA electron beam aimed at the low-Z mask. The electron beam was positioned at different radii and locations around the mask, scanning on the $x = 0$, $y = 0$ and $x = \pm y$ lines, as shown in figure 5.1, to build up a complete picture for particles incident on all parts of the low-Z mask. The data from the stripline signals and the processed signals (using FONT4 analogue processors) were seen on a 4-channel 5 GHz oscilloscope[1] and recorded by the FONT DAQ.

This method was used at low beam charge. The ILC simulations discussed in section 3.4.2 showed that 6.4×10^4 charged particles hit the low-Z mask, delivering 3.5×10^5 GeV of energy. To deliver 3.5×10^5 GeV to the low-Z mask of the FONT module with Method A, the beam charge of the 28.5 GeV beam would have to be 1.2×10^4 electrons per bunch (3.5×10^5 GeV divided by 28.5 GeV). It was decided to use this method between 1×10^4 and 1×10^7 electrons per bunch to match and exceed ILC levels by a few orders of magnitude.

5.2.2 Simulating the experiment: Method A

Method A was simulated in GEANT3 to ensure that the secondary backgrounds it created were similar to those predicted for the IP feedback BPM at the ILC.

The existing GEANT3 model of the FONT module (from chapter 4) was used with an input of 28.5 GeV electrons (generated using a random number generator within Matlab) aimed at a radius of 1.4 cm (x = -1 cm, y = 1 cm) near stripline B. The particles that hit the four striplines were recorded. This simulation was repeated three times.

The energies of these hits for Method A were compared to those from the ILC simulations of the scheme 14, 14 mrad crossing angle with anti-DID. The energy distributions (see figure 5.2) were closely matched with the peak energies both below 1 MeV, confirming that the module combined with electrons on the low-Z mask produces similar secondary backgrounds to the ILC at the striplines.

The ratio of electron, positron and photon hits were remarkably close between the ILC case and Method A case given the difference between the primary pair backgrounds of ILC and the 28.5 GeV electron beam of ESA. The ratios are shown in table 5.2 where striplines

[1]The oscilloscope could be operated in one channel mode with a sampling frequency of 20 GHz.

	A		B		C		
	Striplines	Processors	Striplines	Processors	Striplines		Processors
					In BSY	In ESA	
Energy (GeV)	28.5	28.5	28.5	28.5	28.5	4 - 8	-
Beam Charge (electrons)	$1 \times 10^6 - 1 \times 10^7$	1.5×10^9	1.6×10^{10}	1.6×10^{10}	$4 \times 10^8 - 2 \times 10^{10}$	$1 \times 10^4 - 2 \times 10^6$	-
Beam size	2100 μm $\times$ 700 μm	1300 μm $\times$ 1000 μm	800 μm $\times$ 65 μm	800 μm $\times$ 65 μm	120 μm $\times$ 70 μm	3 cm $\times$ 3 cm	-
Beamline Components	• FONT module • Low current instrumentation		• FONT module • Aluminium foils upstream of module		• FONT module • Very low current instrumentation • Beryllium target in BSY		
General Method	Beam is moved onto low-Z mask creating secondary backgrounds.		Thin radiators are used to produce a halo of low energy particles around the main beam.		A thick radiator in the BSY is used to produce a lot of low energy particles and an energy is selected to transport to ESA.		
Pros	• Creates very large numbers of secondary particles • Can see effect of secondary particles without it being masked by a large signal from the main beam		• Can measure the position of the beam in the presence of backgrounds- a scenario like the ILC.		• Can match the average number and energy density of the ILC on the low-Z mask • Can see effect of secondary particles without it being masked by a large signal from the main beam		
Cons	• Cannot directly compare the effect from the backgrounds to the main signal • Backgrounds are not like those at the ILC in terms of relative number and energy density across the low-Z mask		• Backgrounds are very small compared to the main beam- the signal from the main beam will dominate		• Only average densities are matched, the asymmetry of the ILC backgrounds is not		

Table 5.1: Methods A, B and C for creating backgrounds at ESA are summarised. Some beam parameters are given for each method. They are different depending on whether the data being recorded is the stripline response to the backgrounds or the processor response to the backgrounds and, in the case of Method C, whether the parameters are measured in the beam switchyard (BSY) or in the end station (ESA). The beam sizes for Methods A and B were measured at ESA during the experiment. The beam size for Method C at the BSY is based on measurements by E158 [96]. The method is briefly stated with the pros and cons.

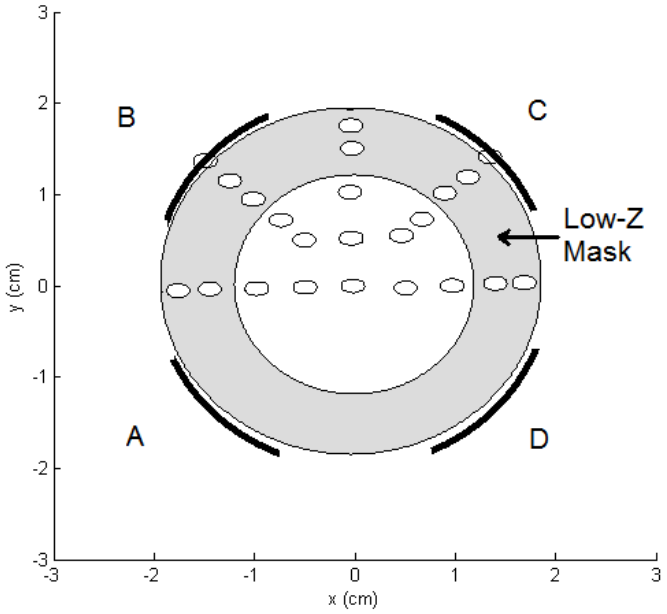

Figure 5.1: The electron beam was placed in the positions on and off the low-Z mask (shaded grey) as indicated above. The striplines are labeled A, B, C and D.

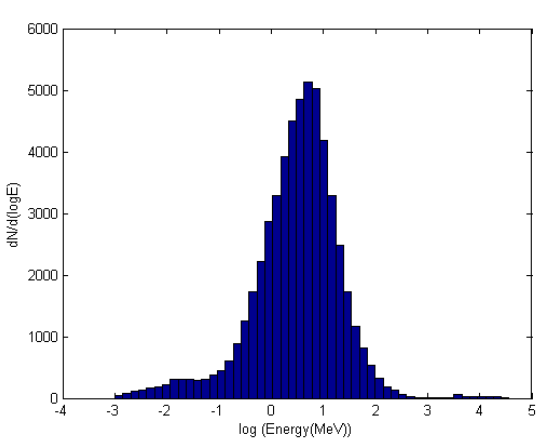

(a) ILC Scheme 14, 14 mrad crossing angle, Anti-DID. 10% of the full simulation.

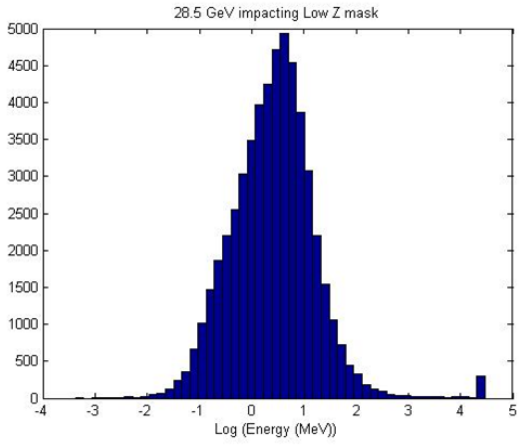

(b) Method A. <1% of the full simulation.

Figure 5.2: Histograms for the energy distribution of charged particle hits on the striplines.

	ILC % of total hits				Method A % of total hits			
	1	2	3	4	A	B	C	D
Electrons	10	14	10	15	6	7	6	6
Positrons	7	8	6	7	3	4	3	4
Photons	83	78	83	78	90	89	90	90

Table 5.2: The percentage of electron, positron and photon hits on each stripline for Method A compared with the percentages for ILC feedback BPM striplines. The striplines are assigned letters as shown in figure 5.1 and numbers as shown in figure 3.24(a). The ILC simulation was for the 14 mrad crossing angle IR, anti-DID and Scheme 14 accelerator parameters.

	A	B	C	D
Electron hits	1.13 ± 0.02	1.41 ± 0.03	1.12 ± 0.01	1.72 ± 0.04
Positron hits	0.60 ± 0.01	0.82 ± 0.04	0.61 ± 0.02	1.00 ± 0.01
Photon hits	16.3 ± 0.9	16.9 ± 0.7	16.1 ± 0.5	25.2 ± 0.8

Table 5.3: The number of particle hits on each stripline for Method A per electron incident on the low-Z mask with a beam offset of r = 1.4 cm (x = -1 cm, y = 1 cm) from a GEANT simulation. The striplines are assigned letters as shown in figure 5.1.

1 and 3 of the ILC feedback BPM and stripline A of the FONT module show the closest match.

The number of electron, positron and photon hits per stripline for Method A are shown in table 5.3 (where hits are given per electron in the ESA beam). Running a beam charge of 1×10^4 electrons, the number of particle hits per stripline are similar to those at the ILC (the ILC numbers are shown in table 3.2 for the 14 mrad crossing angle IR).

5.2.3 Instrumenting the experiment: Method A

This method required instrumentation for low beam currents. Existing beam current monitors did not work below 10^8 electrons per bunch but knowledge of the beam current was required down to 10^4 electrons per bunch. It was also vital to know the position of the beam at larger offsets than the existing ESA BPMs could read so that the beam could be steered onto the low-Z mask (1.2 cm inner radius). The spot size also needed to be measured in order to reproduce the experiment in simulations.

Measuring the beam position

To aid in positioning the beam on the mask, a plastic scintillator block and CCD camera were used. A disused beam profile screen mover a metre upstream of the module (known as 3PR3) had its phosphorescent screen replaced with a block of scintillator. This scintillator

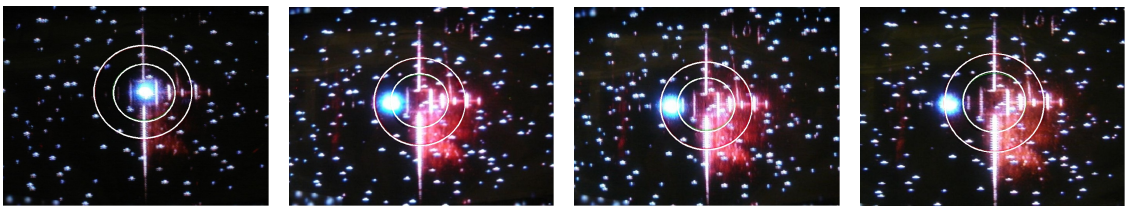

(a) x = 0 cm, y = 0 cm (b) x = -1.25 cm, y = 0 (c) x = -1.5 cm, y = 0 (d) x = -1.75 cm, y = 0

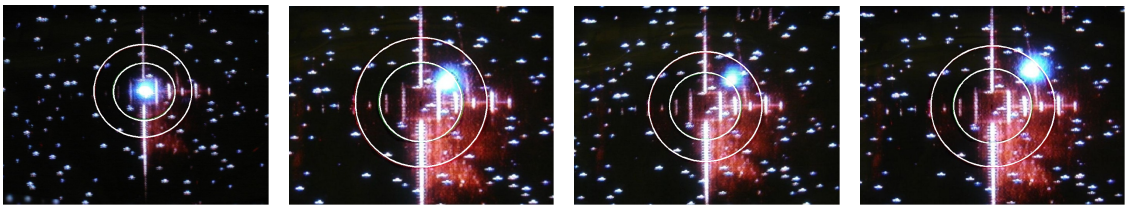

(e) x = y = 0 cm (f) x = y = 0.75 cm (g) x = y = 1 cm (h) x = y = 1.25 cm

Figure 5.3: Photographs of the CCD camera images. The inner radius of the low-Z mask (1.2 cm) is marked as a white circle (the radius is 1.2 cm). The larger white circle marks the inner radius of an upstream collimator (3C1, radius 1.95 cm). The central box in the photos is 1 square centimetre and the major tick-marks on the axes are every 0.5 cm.

produced a lot of scintillator and Cherenkov light[2] when the beam passed through it even at low charge. Mirrors in a periscope formation brought the light from the scintillator to a CCD camera housed in lead bricks about a metre below the beamline. The scintillator screen was marked with axes such that when placed in the beam, the position of the beam could be seen as a bright blue spot (see figure 5.3). The correctors that were used to give the beam a translation in x and y were upstream of a collimator (3C1). This restricted how far on the low-Z mask the beam could be moved to within the inner radius of the collimator (1.95 cm).

A huge drawback to this setup was the poor field of view that could be achieved with the camera and lenses available. Even with the best arrangement, the position of the beam could only be read to within ±0.25 cm. Another issue was that the camera was easily damaged by neutrons. The lead housing minimised this and the CCD camera was removed from the beamline when it was not in use. This made the camera lifetime sufficient for the experiment. The scintillator was susceptible to damage from high intensity beams so the scintillator was only inserted when the beam charge was below 10^7 electrons per bunch and the spot size large.

Measuring the beam spot size

The scintillator light spot was not a good indication of beam spot size so to measure this the normal wire scanners in ESA were used. Although the wire scanner signal could be amplified a little by turning up the voltage on the PMT[3], the beam spot size could not be measured

[2]Cherenkov radiation is caused by the electrons travelling faster than the speed of light in the scintillator material.

[3]Wire scanners involve passing wires across the beam and collecting secondary emission from the interaction in a photomultiplier tube (PMT).

with beam charge lower than 10^9 electrons. The current was raised to do this measurement. This should still give an adequate reading of the size of the beam spot as instabilities that could cause the size to change are only a problem at higher charges [97]. The wire scanner used was 3WS1 and can be seen in figure 4.2.

Measuring the beam charge

The beam charge was measured with three devices to span the range from 10^4 to 10^{10} electrons. An existing toroid at ESA (toroid 4140) operated above 10^8 particles. New toroid electronics were designed [98] to operate below this using a low noise FET as a voltage amplifier. The noise of the system was about 1 mV at the output restricting the operation of this toroid to currents above 1.6×10^5 electrons. The components were saturated just below 10^9 electrons. A third device, a photomultiplier tube and scintillator, was put in place to measure the beam charge below 10^5 electrons.

The low current toroid output (figure 5.4) was sampled by an ADC and read into the ESA DAQ [99] system. The ADC was easily saturated so attenuators were used to bring the signal onto the correct scale. The ADC had a pedestal of 95 counts to be removed from beam charge calculations plus there was a DC offset associated with the input of -30 counts (this was reduced in magnitude when attenuators were placed on the input) making the effective pedestal 65 without any attenuators and 92 with a 20 dB attenuator on the input to the ADC.

The low current toroid was calibrated in two ways.

The first calibration was performed against the existing calibrated toroid (4140) that operated above 10^8 electrons. The ADC window was placed in the second trough of the low current toroid signal as the first trough showed signs of saturation at the higher end of the beam charge used for calibration and the second trough did not. The calibration on toroid 4140 was 10^8 electrons per count so the resolution was poor and there was evidence of some beam charge jitter. Because of this, counts on the low current toroid and counts on the 4140 toroid were recorded over 20 pulses three times at each beam charge setting. This gave a calibration of $(3.0 \pm 0.1) \times 10^4$ electrons per count (see figure 5.5).

The low current toroid was altered in between the two experimental runs so that a calibration current equivalent to 1.35×10^8 electrons could be used to produce a signal in the toroid instead of the beam. An ADC sampled the output signal at a trough as shown in figure 5.4. The low current toroid signal caused by the actual beam current needed to be sampled at the same position in the waveform as the calibration current. According to this method, the calibration constant for sampling at the second trough was $(3.20 \pm 0.06) \times 10^4$ electrons per count. The slight difference from the previous method is due to a different ADC sampling window width. It was preferable to work at the first trough when operating at or below 1.35×10^8 electrons per bunch where there was more sensitivity. Here the calibration was $(2.232 \pm 0.008) \times 10^4$ electrons per count on the ADC.

During the experiment, it was discovered that the stripline signals were too small to be seen above the oscilloscope noise when the beam current was dropped below 10^6 electrons

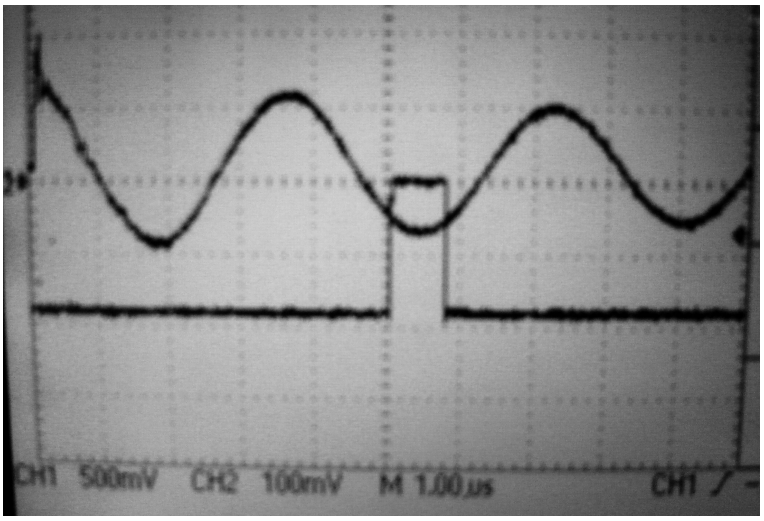

Figure 5.4: Photograph showing the signal of the low current toroid from the calibration current and the ADC window positioned at the second trough.

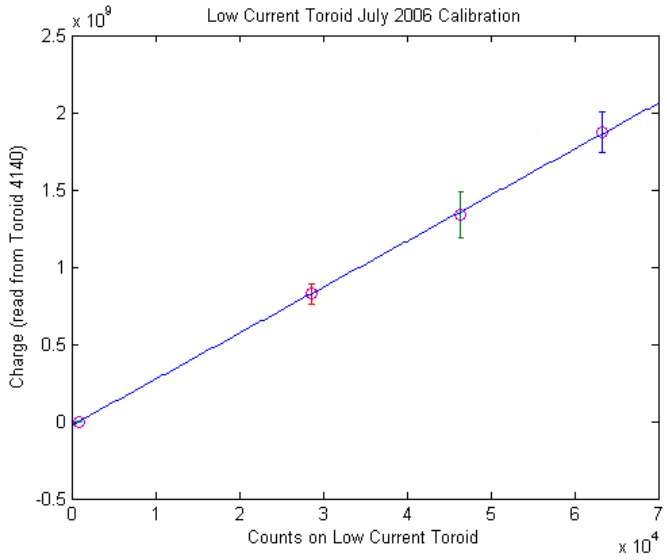

Figure 5.5: The beam charge from toroid 4140 is plotted against the number of counts on the low current toroid. The calibration is beam charge = (counts - pedestal) $\times(3.0 \pm 0.1) \times 10^4$.

per bunch. The photomultiplier, which was positioned to pick up light from the scintillator screen that was used for beam steering, was calibrated against the low current toroid but it was not required.

5.2.4 Performing the experiment: Method A

This method was used during two runs at ESA: July 2006 and March 2007. In July the raw BPM stripline signals were studied and in March the signals were recorded from the FONT4 analogue BPM processors.

Due to concern that a small beam spot would produce a beam too intense for the plastic scintillator, the optics of the standard ESA set-up were changed to make the beam spot larger. This required changing the strengths of two quadrupole magnets. Wire scans confirmed that the beam was 2100 μm in σ_x and 700 μm in σ_y for July 2006 and 1300 μm in σ_x and 1000 μm in σ_y in March 2007.

The beam was steered using upstream dipole correctors x3212 and y3313 using the scintillator and CCD camera to judge the position of the beam at the mask (as described above). The positions steered to are shown in figure 5.1. At each position, the four raw stripline signals from the BPM striplines, brought to the oscilloscope via 200 ft long cables, were recorded in batches of 20 to 100 pulses on the FONT DAQ. As the stripline signals were recorded, the beam charge was recorded through the ESA DAQ. It was necessary to make a beam charge measurement for every position as the beam charge was not stable. Repeat measurements with higher charge were performed to check the relationship between the signals and charge.

In order to see a signal from the striplines on the oscilloscope, the beam charge needed to be at least 1×10^6 electrons. Usually, a beam charge between 10^6 - 10^7 electrons was used. Higher beam charge (1.5×10^9) was required for data taking with the processors as they attenuated the signal further. This meant that the scintillator had to be removed to prevent it from being damaged and the beam had to be steered "blind". Identical magnet settings were used as for the steering with the low charge beam and it was assumed that they moved the high charge beam to the same places. After steering and taking data, the charge was lowered to 1×10^7 and the scintillator used to check the position. It appeared to be slightly low in x but within the already accepted ± 0.25 cm error in positioning the beam.

To bring the beam current down to 10^6 for operation, the method of "boot-strapping" was used whereby the current was lowered until it was half the number of counts on the low current toroid. Attenuation was then removed from the ADC input and the number of counts halved again. In this fashion, the beam current was reduced swiftly to an operating beam current below 10^7 electrons per bunch. The final number of counts was recorded and the exact beam current found with the calibration constant.

When the data with the processors were taken, the processors were set up as described in chapter 2 with a 714 MHz local oscillator. The processors were used after the 200 ft cables for easy and convenient access, not attached locally to the BPM.

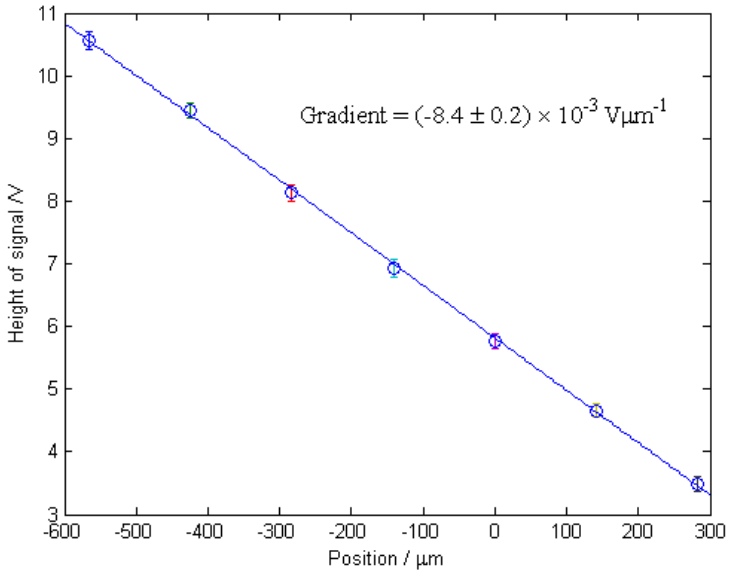

Figure 5.6: The calibration curve for paired/opposing striplines without charge normalisation.

Calibration of the processors and striplines

The stripline and processor signals were calibrated with position. The calibration was achieved using correctors to translate the entire beam in steps of 100 μm. 100 pulses were taken at each point to reduce the effect of the beam charge jitter. The beam charge was 1.5×10^{10} electrons per bunch.

The processor calibration was done using the integrated difference divided by sum as described in section 2.3.2.

The stripline calibration included Fourier interpolation being applied to the data to find the most likely values for the maximum and minimum points of the bipolar stripline signal. Then the difference between the peak to peak magnitude of two paired (i.e. opposing) striplines was calculated and plotted with the position offset to give a calibration constant of 8.4 ± 0.2 mVμm^{-1} (figure 5.6). The calibration curves for the processors and striplines normalised by charge are shown in figures 6.4 and 6.3.

5.3 Results: Method A

5.3.1 Raw stripline response

In July 2006, the stripline response was recorded with the beam positioned at several points on the low-Z mask (see figure 5.1). Due to the azimuthal symmetry of the module, many of these points were equivalent to each other. Essentially, there are two sets of data: one where the beam approaches a stripline along x = y from the centre and another where the beam is moved from the centre along y = 0.

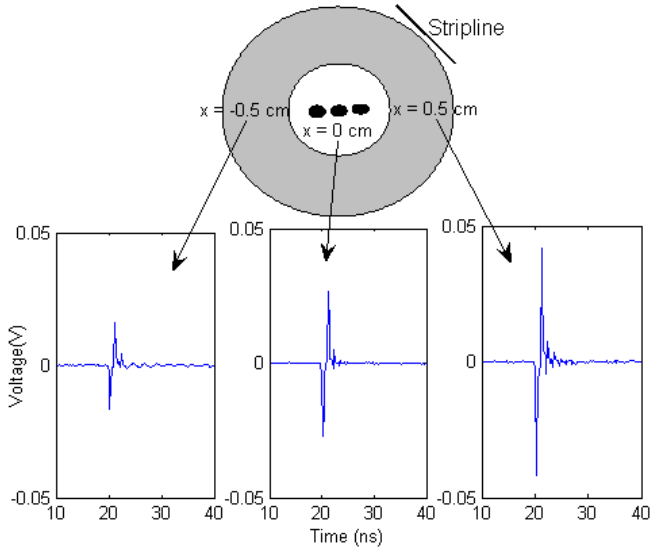

Figure 5.7: Stripline signals in volts from stripline C (see figure 5.1) at three positions on the x axis (x = -0.5 cm, x = 0 cm, x = 0.5 cm). The mean of 20 pulses is shown in each position. The beam charge for x = -0.5 cm is $(1.0 \pm 0.1) \times 10^7$ electrons, x = 0 cm is $(1.5 \pm 0.1) \times 10^7$ electrons and x = 0.5 cm is $(1.8 \pm 0.1) \times 10^7$ electrons.

The beam was moved from the centre of the beampipe to the inner radius of the low-Z mask along y = 0. The stripline response as the beam was moved within the clear beampipe was as expected; as shown in figure 5.7, the signals from the stripline grow in amplitude as the beam approaches the stripline.

Once the beam hit the low-Z mask, the signals from the striplines showed a clear difference. The striplines nearest the beam (C and D as shown in figure 5.1) showed a small change in shape with the negative-going spike of the bipolar signal being smaller in amplitude than the positive-going spike (see figure 5.8). There was a more dramatic response in the striplines on the other side of where the beam was placed (A and B). The amplitude of these signals, shown in figure 5.9, increased when the beam was at x = 1.5 cm and there is a distinct change in the shape of the response with a second negative going signal growing as the beam is moved further onto the mask as well as a DC "hump" between the negative and positive going parts of the usual stripline bipolar signal.

Charge dependence was investigated by moving the beam along y = 0 cm for a beam charge approximately five times higher than used before ($\sim 5 \times 10^7$). This is shown in figure 5.10 for two beam positions where the beam is hitting the low-Z mask. In both cases shown, the higher charge BPM signal is larger by a factor of $\sim$5 which agrees with the beam charge being larger by a factor of $\sim$5. This was true for all positions as the beam was scanned along y = 0 cm, confirming that the shape of the signals was an effect that did not change with charge and that the magnitude scaled linearly with charge.

The beam was also moved along x = $\pm$y. As the striplines of the BPM were rotated by 45°, this path moved the beam directly between one pair of striplines and perpendicular to the other pair (see figure 5.1). As the beam was moved within the clear beampipe, the striplines again behaved as expected with the pair perpendicular to the movement not

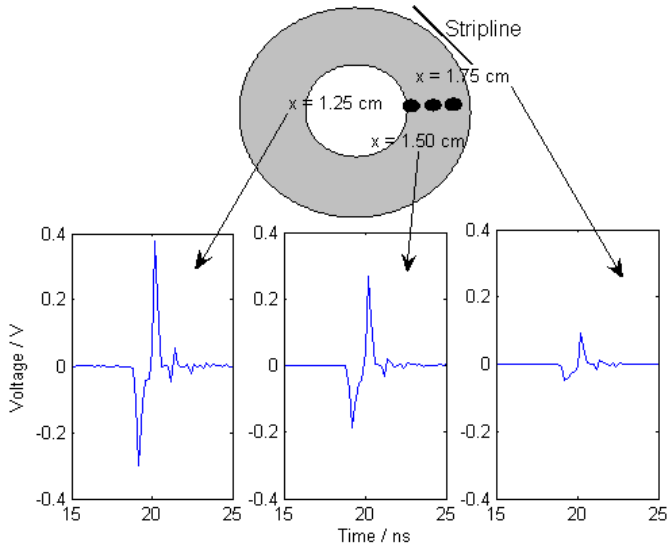

Figure 5.8: Stripline signals in volts from stripline C (see figure 5.1) at three positions on the x axis (x = 1.25 cm, x = 1.5 cm, x = 1.75 cm). The mean of 20 pulses is shown in each position. The beam charge for x = 1.25 cm is $(4.2 \pm 0.5) \times 10^7$ electrons, x = 1.5 cm is $(5.0 \pm 0.3) \times 10^7$ electrons and x = 1.75 cm is $(3.2 \pm 0.4) \times 10^7$ electrons.

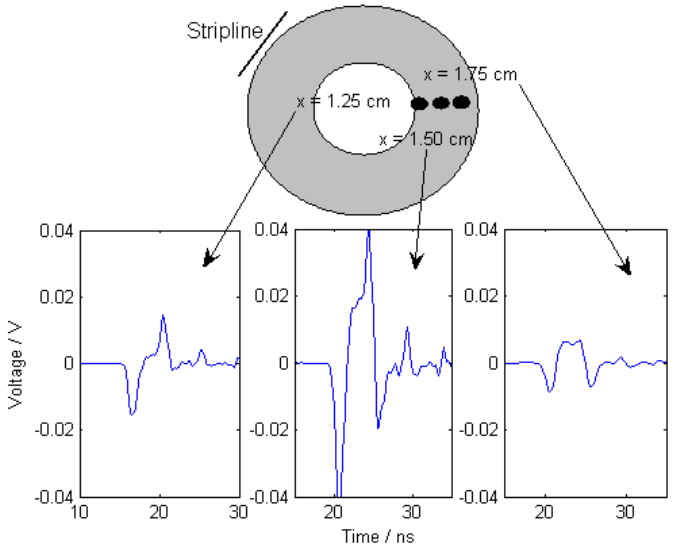

Figure 5.9: Stripline signals in volts from stripline B (see figure 5.1) at three positions on the x axis (x = 1.25 cm, x = 1.5 cm, x = 1.75 cm). The mean of 20 pulses is shown in each position. The beam charge for x = 1.25 cm is $(6.2 \pm 0.8) \times 10^6$ electrons, x = 1.5 cm is $(1.0 \pm 0.1) \times 10^7$ electrons and x = 1.75 cm is $(1.3 \pm 0.1) \times 10^7$ electrons.

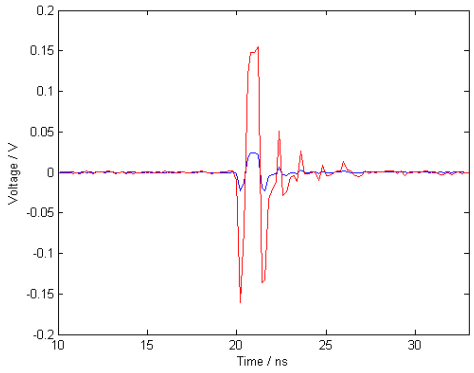

(a) Stripline B signal for the position x = 1.5 cm, y = 0 cm. In blue, the stripline signal at beam charge $(7.9 \pm 0.7) \times 10^6$. In red, the stripline signal at beam charge $(5.0 \pm 0.3) \times 10^7$.

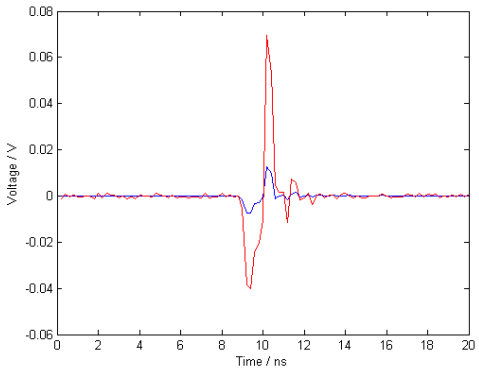

(b) Stripline C signal for the position x = 1.75 cm, y = 0 cm. In blue, the stripline signal at beam charge $(5.5 \pm 0.8) \times 10^6$. In red, the stripline signal at beam charge $(3.2 \pm 0.3) \times 10^7$.

Figure 5.10: Stripline signals at x = 1.5 cm and x = 1.75 cm with different beam charges. The mean of 20 pulses is shown at each charge.

changing, the stripline being approached gaining a larger response and the stripline opposite getting a smaller response. When the beam hit the low-Z mask, all four striplines showed a large response (figure 5.11) due to the increase of charged particle backgrounds. The signals for the perpendicular pair (striplines A and C) showed a small change in shape similar to the striplines in figure 5.8 which also had the beam moving between them rather than directly towards or away. The responses of the targeted stripline (B) and the stripline (D) on the opposite side of where the beam was placed were different: both striplines showed a new second negative-going peak and a "hump' between the first negative-going peak and the positive peak. Stripline B showed the greatest difference from the normal stripline response. The shapes changed for large offsets (see figure 5.12). Both striplines show a similar distortion, with stripline D having the larger second negative-going signal.

It was observed that the stripline signals observed in Method A could be explained qualitatively by secondary emission from the striplines superimposed on the response to charges hitting the striplines and the normal stripline response [100]. The flat positive part in the centre of the signal as seen in figure 5.12, for example, could be explained as secondary emission of electrons occurring along the length of the stripline. The construction of such signals is further discussed in chapter 8.

5.3.2 Processed difference signals

The stripline signals were processed into a difference and sum signal using the FONT4 analogue processors. The beam charge was set at 1.5×10^9 for the use of the processors. The beam was steered similar to before, along y = 0 and x = ±y.

The difference signals grew from zero as the beam was moved towards a stripline in the clear beampipe. When the mask was hit, the stripline responses all increased in amplitude so the sum signal of the processor increased. However, the difference signal did not, leading

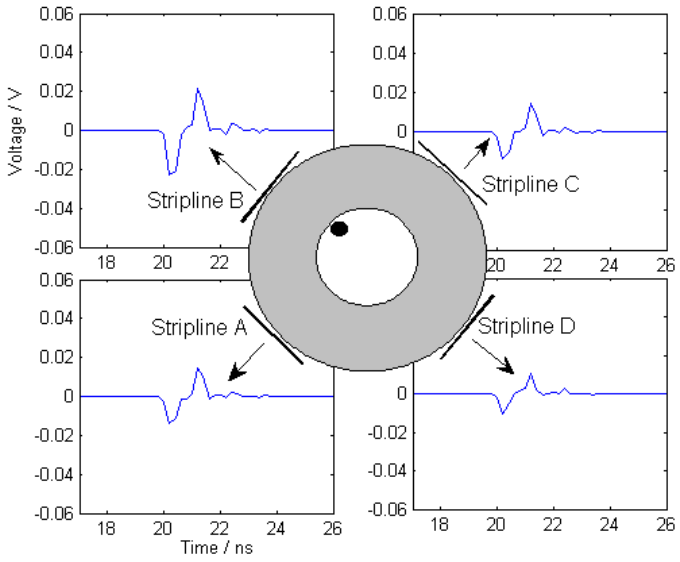

(a) Beam off mask (x = -0.75 cm, y = 0.75 cm). Beam charge is $(7 \pm 1) \times 10^6$ electrons.

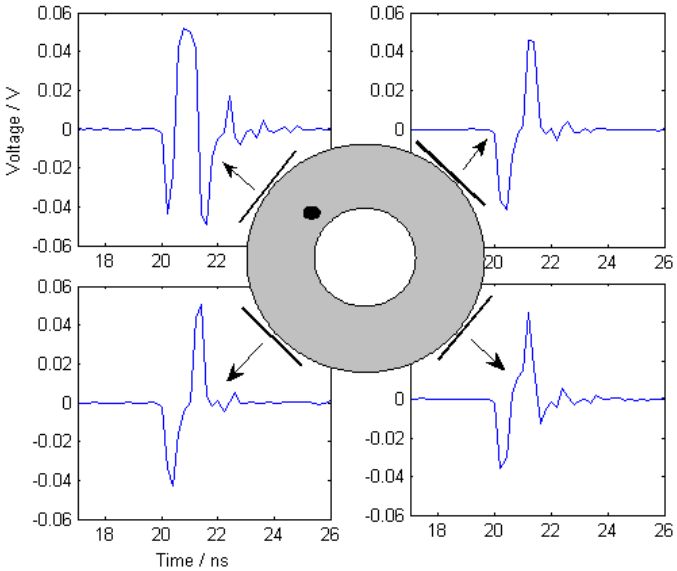

(b) Beam on mask (x = -1 cm, y = 1 cm). Beam charge is $(9 \pm 1) \times 10^6$ electrons.

Figure 5.11: The stripline responses for all four striplines before and after the beam hits the low-Z mask as it is moved along x = -y.

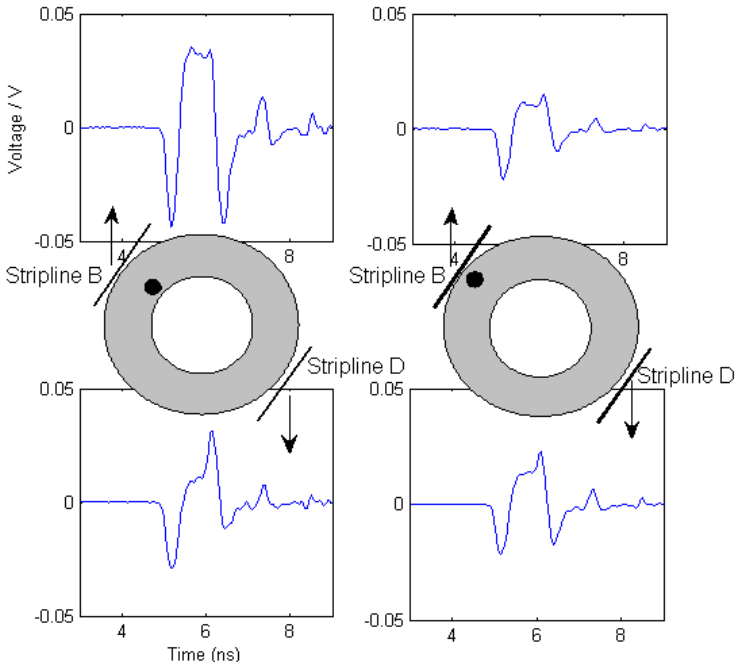

Figure 5.12: Left: Response of two striplines with the beam at x = -1 cm, y = 1 cm (on the low-Z mask) with beam charge $(9 \pm 1) \times 10^6$ electrons. Right: Response of two striplines with the beam at x = -1.25 cm, y = 1.25 cm and beam charge $(4 \pm 1) \times 10^6$ electrons.

to a smaller normalised signal. Even further on the mask, with the beam placed at r = 1.75 cm, the difference signal changed sign (see figure 5.13) showing the processor's sensitivity to the shift between the nearest stripline having the greater signal to the opposite stripline having the greater signal, as shown in figure 5.12.

5.4 ILC Prediction based on Method A

At the ILC all of the low-Z mask is illuminated by particles from the pair backgrounds (figure 3.19). Method A had illuminated spots (approximately 2 mm by 1 mm) on the low-Z mask (figure 5.1). These are two very different scenarios but assuming that the stripline signals from the results of Method A can be summed together, the effect on the striplines from charges hitting at many points around the low-Z mask can be found. For example, figure 5.14 shows two positions (R1 and R2) with the beam placed near striplines in Method A. The stripline signals recorded for the beam at R1 can be added to the stripline signals recorded for the beam in R2 to produce four stripline signals for a situation where particles hit the low-Z mask at the top and at the bottom edges of the low-Z mask.

To a first approximation, this is similar to the ILC case where the particles hitting the low-Z mask are mainly at the top and bottom (see figure 3.25).

Due to rotational symmetry, R1 is equivalent to R2 (which was confirmed in the results from Method A) and in fact only one set of results need be used. In fact, all of the Method

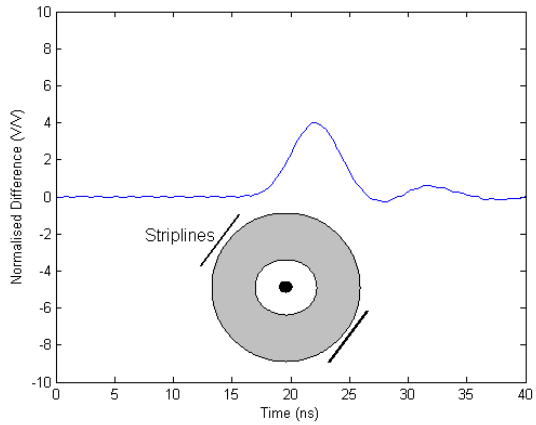

(a) x = 0 cm, y = 0 cm

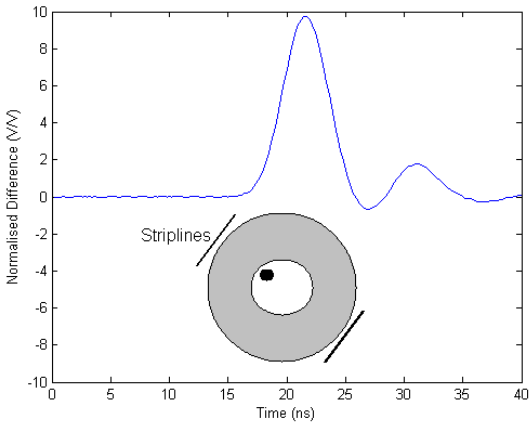

(b) x = -0.75 cm, y = 0.75 cm

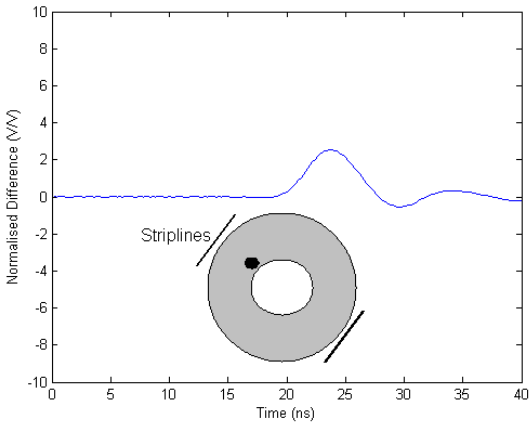

(c) x = -1 cm, y = 1 cm

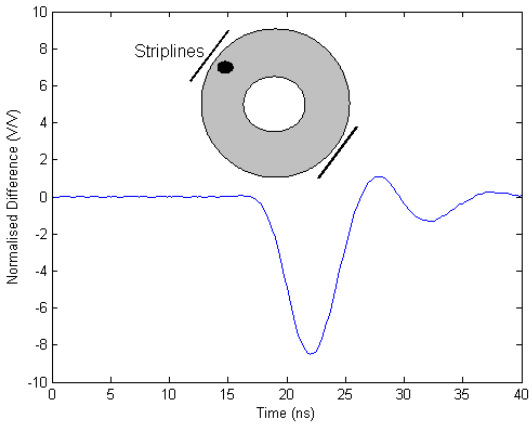

(d) x = -1.25 cm, y = 1.25 cm

Figure 5.13: The response from the FONT4 analogue processor with input signals from striplines B and D. The beam charge was 1.5×10^9 electrons.

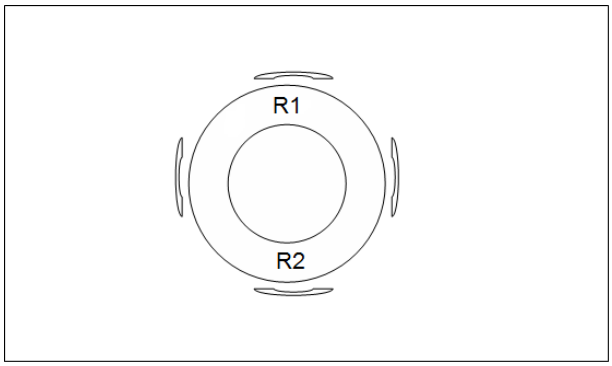

Figure 5.14: Two positions of the Method A beam (R1 and R2). These positions are on the axis between two opposing striplines.



(a) (b)

Figure 5.15: (a): Two positions of the beam (R and X) that were recorded during Method A data taking. (b): R and X extended to cover the entire front face of the module through consideration of rotational symmetry.

A data can be summarised in two positions: runs with the beam aimed along the axis of paired striplines (R) and runs with the beam aimed between two striplines (X) as shown in figure 5.15(a). By considering the rotation of the Method A stripline signals, this is expanded to eight positions (figure 5.15(b)) all of which have associated stripline signals recorded from Method A. Plus, at each R and X, signals were recorded at different radii. In this way, the stripline signals for the illumination of the entire disc of the front face of the low-Z mask can be created.

The simulation of the 14 mrad crossing angle IR with pair backgrounds for the Scheme 14 parameter set was used (section 3.4.4). Each charged electron or positron recorded at the z position of the low-Z mask (285 cm) was associated with stripline signals from R and X: a charged particle in the ILC simulation striking the plane at z = 285 cm on the axis of two opposing striplines was associated with signals from the R set of Method A data (R_{signals}) and a charged particle striking the plane at z = 285 cm on the axis between two adjacent striplines was associated with signals from the X set of Method A data (X_{signals}). Particles falling between these two sets were assumed to create a signal that is a weighted average of R and X using the azimuthal angle ϕ of the particle in the simulation. For example, with $0 < \phi < \frac{\pi}{4}$ the weighted set of signals W_{signals} is:

$$W_{\text{signals}} = \frac{(\frac{\pi}{4} - \phi)}{\frac{\pi}{4}} \times R_{\text{signals}} + \frac{\phi}{\frac{\pi}{4}} \times X_{\text{signals}} \tag{5.1}$$

Four different radii of Method A results were used: 0 cm, 1 cm, 1.5 cm and 1.75 cm. The W_{signals} for a particle was produced using the R_{signals} and X_{signals} from the data set with the radius closest to the radius at which the particle strikes the z = 285 cm plane. The Method A results were divided by the beam charge for that particular set of data so that they were stripline signals for one single charge striking the low-Z mask.

Figure 5.16(a) shows the predicted stripline signals for the ILC IP BPM using this method. Each stripline has a similar predicted signal that is clearly dominated by the pairs that go down the centre of the beampipe since they exhibit the typical bipolar signal

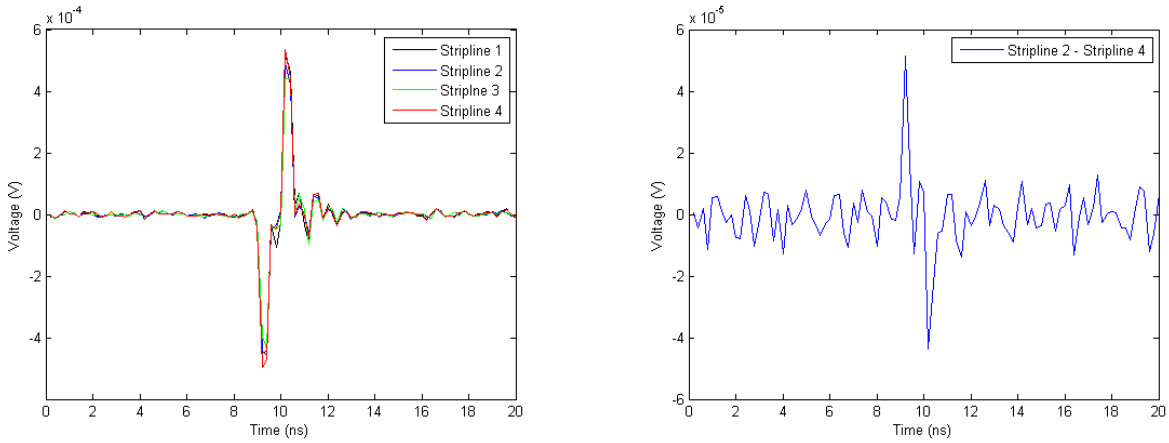

(a) Prediction for the signal on four striplines of the ILC IP feedback BPM.

(b) Prediction for the difference between the top and bottom stripline signals of the ILC feedback BPM.

Figure 5.16: The results for predicting the stripline signals for the ILC IP feedback BPM due to beam-beam pairs based on a weighted sum of Method A stripline signal results.

for charges passing in the beampipe (figure 5.7). The difference between the backgrounds-induced signal on the top stripline and the backgrounds-induced signal on the bottom stripline (stripline 2 subtracted from stripline 1) is shown in figure 5.16(b).

This peak difference of $\sim 5 \times 10^{-5}$ V between the top and bottom stripline due to pair backgrounds is the equivalent to a 6 ± 1 nm offset (from the calibration in figure 5.6). This method of predicting the stripline signals is coarse and taking the difference between two poorly known signals is therefore unreliable. As a more conservative estimate of the position error caused by the pair backgrounds at the ILC, the absolute height of one stripline can be taken ($\sim 5 \times 10^{-4}$ V) with the conclusion that the error is at the very most 60 ± 10 nm.

The main fault in this method is in treating electrons and positrons equally. Although the interactions of electrons and positrons with matter are very similar, the signals for charges passing the upstream end of the stripline are reversed (section 1.5.2). As a result, the amplitude of the predicted signal is overestimated. Given that a 60 nm error is already low enough not to impact the target resolution of 1μm, no further work was done to improve this prediction.

Improvements to this method of predicting ILC signals also include using finer steps in radius and angle. However, this method is always going to be restricted since in approximating the number distribution of charges at the low-Z mask, the energy distribution is not matched.

5.5 Summary to Method A

Method A was developed to produce a lot of secondary backgrounds by directly aiming the beam into the FONT module.

This method involved a low-charge, large-spot size beam scanning the face of the low-Z mask. This required instrumentation at ESA for low beam currents that had to make large movements in x and y.

Simulations of Method A showed a similar energy distribution of electron and positron hits on the striplines. They also showed that the ratio of electron hits to positron hits and photons hits to be close particularly in the case of Method A stripline A and ILC striplines 1 and 3. This can be attributed to the FONT module matching materials and radiation lengths and so creating similar secondary backgrounds regardless of the primary backgrounds.

The results showed raw stripline signals with distorted shapes. Essentially they can be divided into two groups: those that retain the usual bipolar doublet stripline signal (striplines C and D in figure 5.8 and striplines A and C in figure 5.11(b)) and those that show a unique shape with a flat positive central part and two negative-going peaks (striplines B and D in figure 5.12). These shapes can be qualitatively explained by the image charges of electrons passing the upstream end of the stripline and the secondary emission of electrons.

By considering a weighted superposition of the beam spots on the front face of the FONT module in various data runs of Method A, the number density of charged particles at the location of the low-Z mask in the ILC IR was approximated. The GEANT3 simulations of the 14 mrad crossing angle case with anti-DID and Scheme 14 pairs was used for this. Each position of the beam in Method A was associated with stripline signals and so the stripline signals were summed in this weighted superposition, producing a prediction for the ILC. This prediction suggested stripline signals for the IP BPM at the ILC, created by the background pairs, of <0.5 mV in amplitude. This signal produces a <60 nm error in determining position. The prediction is an overestimate due to treating electrons and positrons equally. Also when the difference of the two opposite striplines is taken it will be further reduced.

The predicted degradation in position resolution from the pair backgrounds at the IP is therefore expected to be of the order of nanometres and is not a concern for the goal of micron level resolution.